LETTER

https://doi.org/10.1038/s41586-019-1178-3

Atomic rheology of gold nanojunctions

Jean Comtet[1], Antoine Lainé[1], Antoine Niguès[1], Lydéric Bocquet[1] & Alessandro Siria[1]*

Despite extensive investigations of dissipation and deformation processes in micro- and nano-sized metallic samples[1–7], the mechanisms at play during the deformation of systems with ultimate (molecular) size remain unknown. Although metallic nanojunctions, which are obtained by stretching metallic wires down to the atomic level, are typically used to explore atomic-scale contacts[5,8–11], it has not been possible until now to determine the full equilibrium and non-equilibrium rheological flow properties of matter at such scales. Here, by using an atomic-force microscope equipped with a quartz tuning fork, we combine electrical and rheological measurements on ångström-size gold junctions to study the non-linear rheology of this model atomic system. By subjecting the junction to increasing subnanometric deformations we observe a transition from a purely elastic regime to a plastic one, and eventually to a viscous-like fluidized regime, similar to the rheology of soft yielding materials[12–14], although orders of magnitude different in length scale. The fluidized state furthermore exhibits capillary attraction, as expected for liquid capillary bridges. This shear fluidization cannot be captured by classical models of friction between atomic planes[15,16] and points to an unexpected dissipative behaviour of defect-free metallic junctions at ultimate scales. Atomic rheology is therefore a powerful tool that can be used to probe the structural reorganization of atomic contacts.

Solid metallic materials in the micrometre range and below have been shown to exhibit drastically different mechanical behaviour compared with their macroscopic counterparts. Such size effects originate in the decreasing density of defect-mediated plastic events[1]—such as those occurring during dislocation gliding[2] or twinning[3]—as well as an increasing surface-to-volume ratio[4]. However, extending measurements of the mechanical response of such materials to the 10-nm scale and below has been a challenging task, leading to apparently contradicting reports of both very large yield stress[2,5] and pseudo-elastic deformation[6,7]. Understanding plastic flow and, more generally, dissipation in systems of molecular or atomic sizes has so far remained elusive, despite its fundamental interest and broad applications, which include understanding shape stability in nanoelectronics[17], fundamental dissipation channels in nanomechanical resonators[18] and the role of nanocontacts in macroscopic friction and adhesion[19].

Gold nanojunctions, which are obtained by stretching metallic wires down to the atomic level, have been extensively studied for their electronic properties in the past two decades[8,9] because their molecular dimensions lead to quantized electrical conductance. Here we divert from their standard application and, using a tuning-fork-based atomic force microscope (TF-AFM), we explore the full equilibrium and non-equilibrium rheological flow behaviours of atomic junctions, obtaining insight into the dissipative mechanisms at play in these few-atom systems.

During a typical experiment, a gold electrode, glued on one prong of the TF-AFM, is indented on a gold-coated surface, creating a gold junction (Fig. 1a, b). As observed in Fig. 1c, as the junction thins down because of the increasing distance between the electrode and the substrate, we observe a stepwise variation in the conductance G of the junction, which varies approximately in multiples of $G_0 = e^2/(\pi\hbar) \approx 77\ \mu$S ($e$, electron charge; $\hbar$, reduced Planck constant). Quantization of the conductance occurs as the molecular lateral size of the junction leads to ballistic electronic transport, for which the conductance G is simply proportional to the number N of conductance channels—that is, the number of atoms in the cross-section—with $G \approx NG_0$. This quantization allows direct readout of the transverse dimension of the junction at the single-atom level. Figure 1c shows the successive thinning of the junction from $N = 7$ to $N = 1$ atoms.

To simultaneously probe the mechanical properties of the junction, we further excite the TF-AFM via a piezo dither with a periodic force $F^* = Fe^{i\omega t}$ of amplitude F and frequency ω (t, time), leading to subnanometric oscillations $a^* = ae^{(i\omega t + \phi)}$ of the tuning fork and upper gold electrode, with ϕ the phase shift between forcing and oscillations. The viscoelastic behaviour of the gold nanojunction can be characterized by the complex impedance $Z^* = F^*/a^* = F/ae^{-i\phi}$, where the real $Z' = \mathrm{Re}(Z^*)$ and imaginary $Z'' = \mathrm{Im}(Z^*)$ parts characterize the conservative (elastic) and dissipative responses of the junction, respectively (see Fig. 1a and Methods section 'Measurement of viscoelastic properties').

In Fig. 1d we show the variations of Z' and Z'', measured with a fixed oscillation amplitude of $a = 70$ pm, along with the variation of the junction conductance during elongation (Fig. 1c). On each plateau in the conductance plot, the stiffness Z' is approximately constant, indicating a constant mechanical structure of the junction, whereas the dissipative modulus Z'' is vanishingly small, suggesting the absence of intrinsic dissipation in the structure for such deformations. For each change in conductance, we observe a transient decrease in stiffness Z' and a slight increase in dissipation Z'' (red arrows in Fig. 1d), which can be interpreted as signatures of plastic reorganization during the transformation between states of different contact size. These measurements are consistent with previous measurements on metallic junctions, which reported that elongation is caused by successive elastic and yielding events, concomitant with changes in the electrical conductance[5,10,11,20].

Going beyond this simple picture requires a distinct strategy to probe the full non-equilibrium rheological flow properties and dissipative mechanisms at play in the junction. Our methodology involves maintaining a fixed number of atoms in the cross-section through feedback control of the junction conductance G and subjecting the junction to increasing shear to probe its viscoelastic flow properties under a wide range of shear rates and stresses (with shear amplitude ranging from 20 pm to 1 nm; see Extended Data Fig. 5). This approach is similar in spirit—although at a radically different length scale—to the exploration of the mechanical response of foams and emulsions[12,13], and allows the direct measurement of the rheological response at the atomic scale.

As shown in Fig. 2a for $N = 11$ atoms, the fluctuations in the dimensionless conductance trace $N = G/G_0$ increase at large oscillation amplitude, but the mean contact conductance—and thus the average junction geometry—remains fixed. As shown in Fig. 2b, simultaneous measurements of the elastic ($Z' = \mathrm{Re}(Z^*)$; black) and dissipative ($Z'' = \mathrm{Im}(Z^*)$; red) parts of the mechanical impedance Z^* allow the extraction of the full linear and nonlinear rheological flow properties of the junction. Three consecutive regimes are observed as a function of oscillation amplitude: elastic, plastic and liquid-like behaviour. Remarkably, despite a scale difference of orders of magnitude, this

[1]Laboratoire de Physique de l'Ecole Normale Supérieure, ENS, Université PSL, CNRS, Sorbonne Université, Université Paris-Diderot, Sorbonne Paris Cité, UMR CNRS 8550, Paris, France.
*e-mail: alessandro.siria@lps.ens.fr

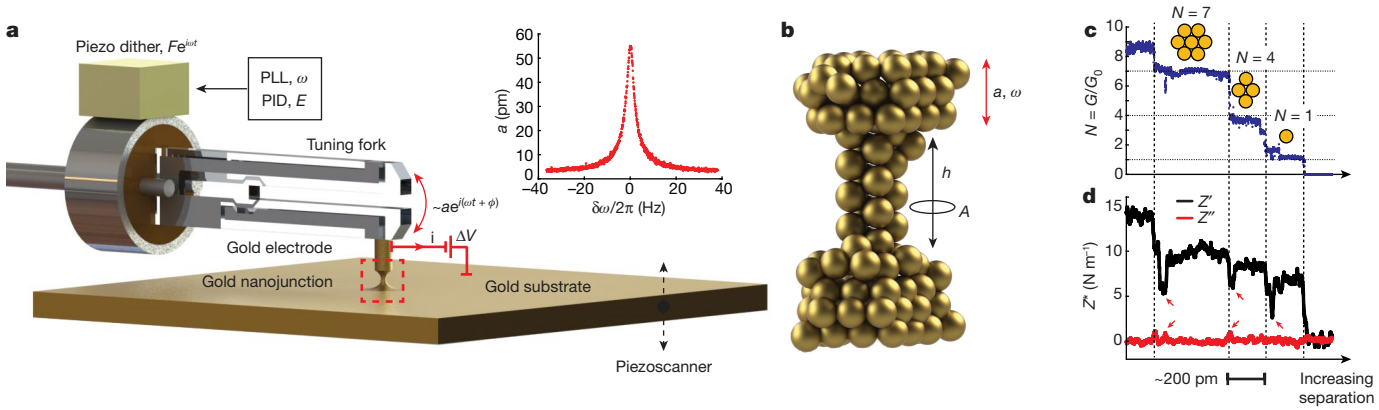

Fig. 1 | Experimental setup. a, Schematic of the experimental setup. A quantum point contact, consisting of a gold nanojunction (red dashed box), is formed between a gold electrode attached to the tuning fork and a gold substrate. A bias ΔV is applied between the electrode and the substrate, allowing measurements of the junction conductance, G. The position of the gold substrate is controlled with a piezoscanner. A piezo dither excites the tuning fork with an oscillatory force $F^* = Fe^{i\omega t}$, leading to the oscillation $a^* = ae^{i(\omega t+\phi)}$ of the gold electrode and the tuning fork. Two feedback loops tune the excitation frequency ω (phase-locked loop, PLL) and excitation force F (proportional integral derivative controller, PID) to systematically excite the tuning fork at resonance and maintain a set oscillation amplitude, allowing the direct measurement of the viscoelastic impedance $Z^* = F^*/a^*$ of gold nanojunction (see Methods section 'Measurement of viscoelastic properties'). Inset, resonance curve of the free tuning fork in air. $\delta\omega$, shift of the tuning-fork resonance frequency. **b**, Schematic representation of the idealized junction geometry for $N = G/G_0 \approx 4$. The junction is assumed to have a rod-like shape with height h and surface area $A \approx N\pi d_0^2/4$. **c**, Typical conductance trace for increasing separation between the gold electrode and the gold substrate. The conductance varies stepwise in multiples of G_0. **d**, Simultaneous measurement of the conservative (Z'; black) and dissipative (Z''; red) part of the mechanical impedance Z^* of the gold junction, here in the low-amplitude (elastic) regime. Red arrows indicate transient decrease in stiffness Z' and increase in dissipation Z'', which are interpreted as signatures of plastic reorganization of the junction.

overall phenomenology echoes similar trends for plastic flows in soft yielding materials[12,13].

At low oscillation amplitude, the gold junction is unperturbed, and we observe a purely elastic response, characterized by the absence of dissipation in the junction ($Z'' \approx 0$) and a finite positive stiffness $Z' > 0$ (green region in Fig. 2b). Accordingly, current fluctuations are found to be small (see Fig. 2a, green histogram with spectral density $S_N = 0.01\ \mathrm{Hz}^{-1/2}$, which is defined in terms of the distribution of N as $S_N = \sigma/\sqrt{\nu}$, where ν is the sampling frequency and σ the standard deviation). The constant elastic stiffness Z'_0 in the elastic regime allows a coarse characterization of the contact height h (Fig. 1b) which is found typically in the range $h \approx 1$–6 nm (see Methods section 'Geometry of the junction').

As shown in Fig. 2b, increasing the oscillation amplitude a for a fixed contact size N, we observe an abrupt decrease in the stiffness Z' and a corresponding increase in the dissipative response Z'' (going from the green to the red zone in Fig. 2b; we note that the rheological curves are completely reversible upon decrease of the shear rate—see Extended Data Fig. 6). This dramatic change points to a dissipative reorganization of the junction under shear, which is further evidenced by the increase in current fluctuations (Fig. 2a; red histogram with spectral density $S_N = 0.01\ \mathrm{Hz}^{-1/2}$). This mechanical response is in striking analogy to the (nonlinear) rheology of soft yielding materials, such as foams and emulsions[12,13], where it is a signature of the onset of yielding and plasticity. Here this regime occurs above a threshold oscillation amplitude a_Y, which we define as the point where Z'_0 decreases and Z''_∞ increases to half their asymptotic values ($Z'(a_Y) \approx Z'_0/2$, roughly concomitant to $Z''(a_Y) \approx Z''_\infty/2$; alternative definitions give similar results).

Using the quantized variation of the junction conductance with the lateral number of atoms ($G = NG_0$), we now vary—atom by atom—the lateral size of the junction, from sizes of $N \approx 30$ atoms down to $N \approx 3$ atoms, corresponding to an equivalent cross-sectional area of $A \approx N\pi d_{\mathrm{gold}}^2/4 \approx 2 - 0.2\ \mathrm{nm}^2$, where $d_{\mathrm{gold}} = 0.288$ pm is the atomic diameter of gold (Extended Data Fig. 5). As shown in Fig. 3a, the yield force, defined as $F_Y = Z'_0 a_Y$, is roughly proportional to the mean number N of atoms in a cross-section (lower axis) or equivalently the cross-sectional area A (upper axis).

The corresponding yield stress $\sigma_Y = F_Y/A$ is accordingly found to be roughly independent of the contact area and of the order of 5 GPa (Fig. 3b, left axis), whereas the yield strain $\varepsilon_Y = a_Y/h = \sigma_Y/E_{\mathrm{gold}}$ is found to be 5%–10%, where E_{gold} is the Young modulus of bulk gold (Fig. 3b, right axis; see Methods section 'Geometry of the junction').

Importantly, these values are much larger than those in macroscopic gold samples, for which σ_Y ranges[21] from 55 to 200 MPa, or in single-crystal gold nano-pillars, where σ_Y is of the order of[22] 500 MPa. Such high values of yield stress and yield strain are consistent with the expected absence of defects in atomic-size junctions.

As a first modelling approach, one may compare the values of the experimental yield stress to a Frenkel-type estimate[11,15,16] on the basis of the slippage of a perfect crystal (Fig. 3c). For slip along the {111} plane of an fcc crystal, the resolved shear stress is given by $\tau_{\max} \approx G/9$. By taking a gold shear modulus of $G = 27$ GPa and a Schmid factor of $m \approx 0.5$, we find a yield stress of $\sigma_Y \approx \tau_{\max}/m \approx 6$ GPa, in good agreement with our measurements (Fig. 3b). This confirms that the junction yields merely as a defect-free ordered crystal, which is to be expected for such size.

An important objective is to understand the influence of shear stress and shear rate on the observed plastic transition. To probe this dependence, we subject the junction to additional oscillatory strains at various frequencies, as sketched in Fig. 3d. Here, plastic flow is induced by this external shear while the junction properties are simultaneously probed with the TF-AFM oscillating at a constant amplitude (see Methods section 'Effect of excitation frequency on the plastic transition' and Extended Data Fig. 3). Such experiments are similar in spirit to superposition rheometry[23]. As shown in Fig. 3e, these complementary measurements demonstrate that the yield strain for the plastic transition is basically independent of the frequency of the oscillatory strain. The plastic transition is accordingly driven by a critical strain, and not by a critical strain rate, as expected for a system with no intrinsic timescales.

Looking into the details of the $\sigma_Y(N)$ and $\varepsilon_Y(N)$ curves, one may remark that the yield strain and yield stress appear to exhibit local maxima for a number of specific values of the conductance channel number N, typically $N \approx 6$, 12, 14, 23. Interestingly these values are close to the (so-called) 'magic' numbers of the more stable gold wires, which have been predicted theoretically[24] to be $N \approx 7$, 11, 14–15, 23 and have been observed using a transmission electron microscope[25]. This would suggest that the more stable gold wires require a larger yield

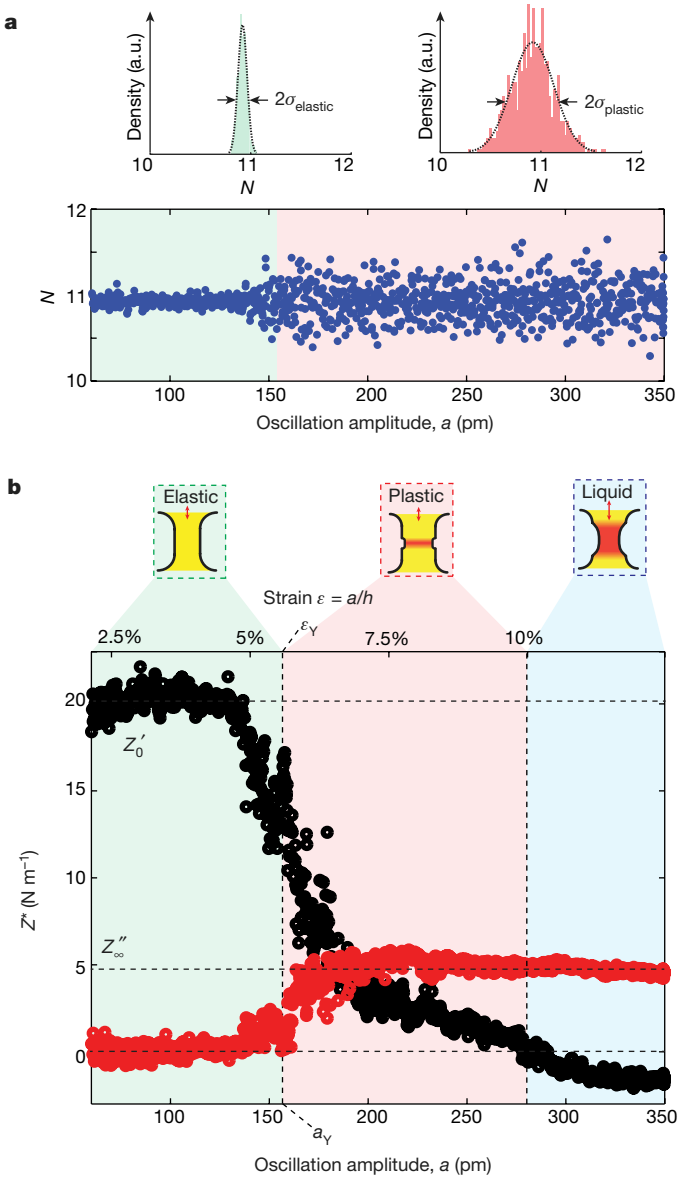

Fig. 2 | Atomic rheology. a, Bottom, dimensionless conductance trace, $N = G/G_0$, as a function of the oscillation amplitude of the TF-AFM for a sampling rate of 50 Hz. At the transition between the elastic and plastic deformation regimes, the current noise increases while N retains a fixed mean value. Top, histograms show the current distribution for the elastic (green, left) and plastic (red, right) regimes and the corresponding distribution width σ. a.u., arbitrary units. **b**, Measurement of the viscoelastic properties of the junction with a fixed cross-sectional area. The variation of the conservative (Z'; black) and dissipative (Z''; red) mechanical impedance of the junction is shown as a function of the oscillation amplitude a of the TF-AFM. With increasing oscillation amplitude, we observe a successive transition from the elastic (green; constant $Z' = Z'_0$, $Z'' = 0$) to the plastic regime (red; decrease in Z', increase in Z'' to a plateau at Z''_∞), up to a liquid-like regime showing capillary adhesion (blue; $Z' < 0$).

strain to enter the plastic regime. This observation, however, deserves a dedicated exploration, which we leave for future work.

We now turn to the regime of large deformations (Fig. 2b, red zone). Surprisingly, the dissipative modulus exhibits a plateau in this regime and thus becomes independent of the imposed deformation a, while the junction stiffness decreases steadily (Fig. 2b). The corresponding dissipative force is accordingly expected to increase linearly with deformation, as $F_D \approx Z''_\infty a$, suggesting a 'viscous-like' dissipation, for which the dissipation is proportional to the imposed velocity, with a linear response between driving and dissipation. One would accordingly expect $F_D = \eta\dot{\gamma}A$, with $\dot{\gamma} \approx a\omega/h \approx 10^4\ \mathrm{s}^{-1}$ the typical shear rate, A the contact area and η the material viscosity.

To further assess these concepts, we plot in Fig. 4a the friction coefficient $F_D/\dot{\gamma}$ (defined as $F_D/\dot{\gamma} = Z''_\infty h/\omega$) as a function of the contact lateral size N (lower axis) or cross-section A (upper axis). This plot confirms that the dissipative force is proportional to the contact area, allowing us to infer the viscosity η (Fig. 4b), which is found to be roughly constant at about $\eta \approx 7 \times 10^4$ Pa s at the TF-AFM excitation frequency of $\omega_{TF}/2\pi \approx 31$ kHz. This viscous-like regime is completely unexpected for defect-free crystalline systems (Fig. 2c), for which plastic flow should occur at constant stress[15,16] (see Methods section 'Comparison with Prandtl–Tomlinson model' and Extended Data Fig. 7).

To obtain further insight into this viscous-like behaviour, one may define a Maxwell timescale τ_M characterizing the relaxation of the system as $\eta = G_{gold}\tau_M$ with $G_{gold} = 27$ GPa the shear modulus of gold[13]. The corresponding value of $\tau_M \approx 3\ \mu$s is huge compared to microscopic timescales (typically in the picosecond range) and very close to the excitation timescale of about $1/\omega_{TF} = 5\ \mu$s. This therefore suggests that the excitation does set the relaxation timescale of the junction under strong deformation, in line with the behaviour of yielding materials (such as emulsions, foams or granular materials), where the fluidity (inverse viscosity) is fixed by the excitation timescale itself[14,26,27].

To assess this dependence of the viscous behaviour on the excitation frequency, we measure the viscosity η of the liquefied gold junction that is induced by an additional excitation frequency ω_s (see Fig. 3c, Methods section 'Effect of excitation frequency on the plastic transition' and Extended Data Fig. 2). As shown in Fig. 4c, the measured viscosity is found to be roughly independent of the excitation frequency for $\omega_s/\omega_{TF} < 1$, as the response of the junction is accordingly fixed by the lowest excitation time, $1/\omega_{TF}$. For larger excitation frequency, $\omega_s/\omega_{TF} > 1$, we observe a thinning behaviour with $\eta \approx \eta_{TF}(\omega_s/\omega_{TF})^{-\alpha}$, where $\alpha \approx 0.28$ and $\eta_{TF} \approx 7 \times 10^4$ Pa s. This thinning behaviour further highlights the dominant role of the excitation frequency in the liquid-like dissipative behaviour of the junction.

Our experiments thus point to unexpected dissipation channels during the deformation of the junction under large strain. Keeping in mind the yielding process in macroscopic soft materials[13,14], such fluidization under stress might be due to the collective atomic reconstruction process, potentially favoured by the rapid surface diffusion of gold atoms[6,7,28,29]. Such additional dissipation channels—completely unexpected for dislocation-free ordered crystalline systems—offer an exciting perspective for the fundamental modelling of dissipative processes at the atomic scale. Finally, the slight deviation from linearity observed for $N > 20$ in Figs. 3a, 4a suggests a possible transition to more traditional dislocation-based mechanisms as sample volumes become sufficiently large.

Surprisingly, the liquid-like character of the gold junction is also recovered in the conservative elastic response in the form of a negative stiffness under large strain (Fig. 2b, blue zone). This regime is therefore associated with an attractive adhesive response of the junction, which is reminiscent of capillary adhesion in macroscopic capillary bridges[30] (Fig. 4d). This additional signature of the liquid-like behaviour of the junction at large oscillation amplitudes, whose conservative mechanical response becomes dominated by surface effects, is further confirmed by additional force spectroscopy measurements in vacuum, showing a 'jump to contact' of the liquified gold (see Methods section 'Capillary attraction at large oscillation amplitude' and Extended Data Fig. 3). Order-of-magnitude estimates of local junction heating discard frictional heating as being responsible for the observed adhesive behaviour of the junction (see Methods section 'Energy balance for the shear-induced fluidization of the junction' and Extended Data Fig. 4).

These observations allow us to estimate the surface stress of the liquefied gold meniscus. Using the expression for the adhesive force induced by a perfectly wetting liquid between two spherical contacts, we get a stiffness of $Z' \approx -2\pi\gamma(R/h)$ (Fig. 4d)[30]. By identifying the radius R with that of the cross-sectional area of the bridge (Fig. 2b), we

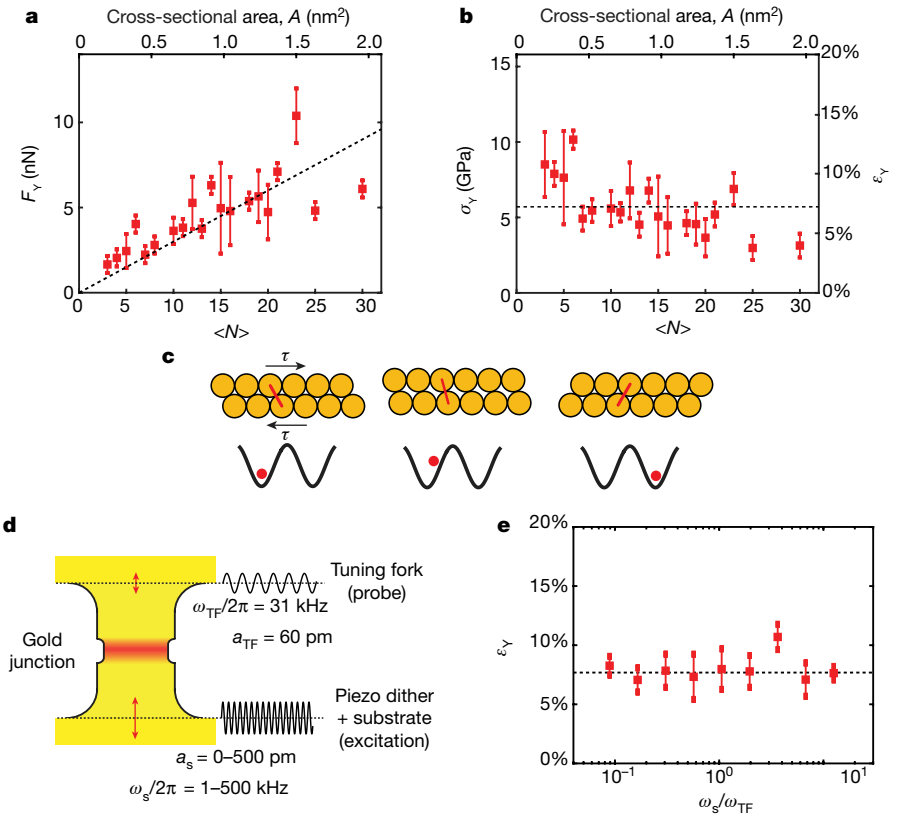

Fig. 3 | Yielding threshold. a, Yield force, F_Y. **b**, Yield stress σ_Y (left axis) and yield strain ε_Y (right axis) as a function of cross-sectional atom number N (and surface area A of the junction; upper axis). **c**, Slip in a perfect crystal between two atomic planes under shear stress τ. **d**, Schematic of the setup. An additional piezo dither is placed below the substrate, allowing to shear the junction at an additional frequency $\omega_s/2\pi$, while the junction properties are simultaneously probed by the TF-AFM (see Methods section 'Effect of excitation frequency on the plastic transition'). **e**, Yield strain ε_Y as a function of the additional excitation frequency ω_s (respective to the TF-AFM frequency ω_{TF}) for $N = 15$. Error bars represent one standard deviation and are taken to be 10% for single-valued points.

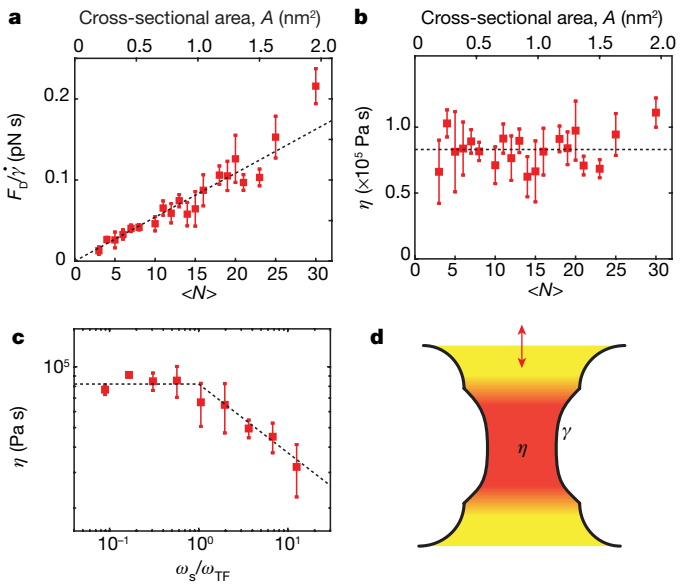

Fig. 4 | Liquid-like behaviour. a, Dissipative hydrodynamic force $F_D/\dot{\gamma}$, with $\dot{\gamma} = a\omega/h$ as a function of cross-sectional atom number N (and surface area of the junction; upper axis). **b**, Viscosity η as a function of N. **c**, Measured viscosity as a function of oscillation frequency ω_s/ω_{TF} for $N = 15$. Error bars are one standard deviation and are taken to be 10% for single-valued points. **d**, Liquid-like response of the junction at large deformation, with signatures of both viscous-like dissipation (viscosity η) and capillary adhesion (surface tension γ).

find that, for the experiment of Fig. 2, $R/h \approx 0.17$ and $Z' \approx -2$ N m^{-1}, leading to an estimate of the surface stress of $\gamma \approx 2$ N m^{-1}. This value is in fair agreement with the expected value of 1 N m^{-1} for the surface tension of liquid gold[31].

Altogether our study enables the first investigation of the full equilibrium and non-equilibrium atomic rheology of a gold junction with single-atom resolution. Our measurements highlight a counter-intuitive fluidization of the gold junction under large imposed deformation, akin to soft-matter yielding materials. Ultimately, fluidization leads to the complete liquid-like response of the junction under large deformation, with signatures of both viscous-like dissipation and capillary-like adhesion. Such a viscous-like response is not captured by standard mechanical models of crystalline interfaces and would require a full description of the atomic reconstruction under the imposed stress as a supplementary feature. This offers new perspectives in the modelling of defect-free metallic materials and echoes recent simulations of bulk metal plasticity at large strains[32]. Finally, these experiments could find interesting applications in the context of ultrasonic and cold welding[33] and enable a better understanding of macroscopic friction on the basis of individual atomic-contact mechanics[19].

Online content

Any methods, additional references, Nature Research reporting summaries, source data, statements of data availability and associated accession codes are available at https://doi.org/10.1038/s41586-019-1178-3.

Received: 21 September 2018; Accepted: 1 March 2019;
Published online: 08 May 2019

1. Kraft, O., Gruber, P. A., Mönig, R. & Weygand, D. Plasticity in confined dimensions. *Annu. Rev. Mater. Res.* **40**, 293–317 (2010).

2. Wu, B., Heidelberg, A. & Boland, J. J. Mechanical properties of ultrahigh-strength gold nanowires. *Nat. Mater.* **4**, 525–529 (2005).
3. Yu, Q. et al. Strong crystal size effect on deformation twinning. *Nature* **463**, 335–338 (2010).
4. Chen, C. Q., Shi, Y., Zhang, Y. S., Zhu, J. & Yan, Y. J. Size dependence of Young's modulus in ZnO nanowires. *Phys. Rev. Lett.* **96**, 075505 (2006).
5. Rubio, G., Agraït, N. & Vieira, S. Atomic-sized metallic contacts: mechanical properties and electronic transport. *Phys. Rev. Lett.* **76**, 2302–2305 (1996).
6. Kuipers, L. & Frenken, J. W. M. Jump to contact, neck formation, and surface melting in the scanning tunneling microscope. *Phys. Rev. Lett.* **70**, 3907–3910 (1993).
7. Sun, J. et al. Liquid-like pseudoelasticity of sub-10-nm crystalline silver particles. *Nat. Mater.* **13**, 1007–1012 (2014).
8. Yanson, A. I., Rubio Bollinger, G., van den Brom, H. E., Agraït, N. & van Ruitenbeek, J. M. Formation and manipulation of a metallic wire of single gold atoms. *Nature* **395**, 783–785 (1998).
9. Ohnishi, H., Kondo, Y. & Takayanagi, K. Quantized conductance through individual rows of suspended gold atoms. *Nature* **395**, 780–783 (1998).
10. Shiota, T., Mares, A. I., Valkering, A. M. C., Oosterkamp, T. H. & van Ruitenbeek, J. M. Mechanical properties of Pt monatomic chains. *Phys. Rev. B* **77**, 125411 (2008).
11. Agraït, N., Yeyati, A. L. & van Ruitenbeek, J. M. Quantum properties of atomic-sized conductors. *Phys. Rep.* **377**, 81–279 (2003).
12. Mason, T. G., Bibette, J. & Weitz, D. A. Yielding and flow of monodisperse emulsions. *J. Colloid Interface Sci.* **179**, 439–448 (1996).
13. Larson, R. G. *The Structure and Rheology of Complex Fluids* (Oxford University Press, New York, 1999).
14. Bocquet, L., Colin, A. & Ajdari, A. A kinetic theory of plastic flow in soft glassy materials. *Phys. Rev. Lett.* **103**, 036001 (2009).
15. Frenkel, J. Zur Theorie der Elastizitätsgrenze und der Festigkeit kristallinischer Körper. *Z. Phys.* **37**, 572–609 (1926).
16. Zaloj, V., Urbakh, M. & Klafter, J. Atomic scale friction: what can be deduced from the response to a harmonic drive? *Phys. Rev. Lett.* **81**, 1227–1230 (1998).
17. Lu, W. & Lieber, C. M. Nanoelectronics from the bottom up. *Nat. Mater.* **6**, 841–850 (2007).
18. Güttinger, J. et al. Energy-dependent path of dissipation in nanomechanical resonators. *Nat. Nanotechnol.* **12**, 631–636 (2017).
19. Persson, B. N. J., Albohr, O., Tartaglino, U., Volokitin, A. I. & Tosatti, E. On the nature of surface roughness with application to contact mechanics, sealing, rubber friction and adhesion. *J. Phys. Condens. Matter* **17**, R1–R62 (2005).
20. Marszalek, P. E., Greenleaf, W. J., Li, H., Oberhauser, A. F. & Fernandez, J. M. Atomic force microscopy captures quantized plastic deformation in gold nanowires. *Proc. Natl Acad. Sci. USA* **97**, 6282–6286 (2000).
21. Espinosa, H. D., Prorok, B. C. & Peng, B. Plasticity size effects in free-standing submicron polycrystalline FCC films subjected to pure tension. *J. Mech. Phys. Solids* **52**, 667–689 (2004).
22. Lee, S. W., Han, S. M. & Nix, W. D. Uniaxial compression of fcc Au nanopillars on an MgO substrate: the effects of prestraining and annealing. *Acta Mater.* **57**, 4404–4415 (2009).
23. Vermant, J., Moldenaers, P., Mewis, J., Ellis, M. & Garritano, R. Orthogonal superposition measurements using a rheometer equipped with a force rebalanced transducer. *Rev. Sci. Instrum.* **68**, 4090–4096 (1997).
24. Tosatti, E., Prestipino, S., Kostlmeier, S., Dal Corso, A. & Di Tolla, F. D. String tension and stability of magic tip-suspended nanowires. *Science* **291**, 288–290 (2001).
25. Kondo, Y. & Takayanagi, K. Synthesis and characterization of helical multi-shell gold nanowires. *Science* **289**, 606–608 (2000).
26. Eisenmann, C., Kim, C., Mattsson, J. & Weitz, D. A. Shear melting of a colloidal glass. *Phys. Rev. Lett.* **104**, 035502 (2010).
27. Dijksman, J. A., Wortel, G. H., van Dellen, L. T. H., Dauchot, O. & van Hecke, M. Jamming, yielding, and rheology of weakly vibrated granular media. *Phys. Rev. Lett.* **107**, 108303 (2011).
28. Gosvami, N. N. et al. Ageing of a microscopic sliding gold contact at low temperatures. *Phys. Rev. Lett.* **107**, 144303 (2011).
29. Merkle, A. P. & Marks, L. D. Liquid-like tribology of gold studied by in situ TEM. *Wear* **265**, 1864–1869 (2008).
30. Crassous, J., Charlaix, E. & Loubet, J.-L. Nanoscale investigation of wetting dynamics with a surface force apparatus. *Phys. Rev. Lett.* **78**, 2425–2428 (1997).
31. Kaufman, S. M. & Whalen, T. J. The surface tension of liquid gold, liquid tin, and liquid gold-tin binary solutions. *Acta Metall.* **13**, 797–805 (1965).
32. Zepeda-Ruiz, L. A., Stukowski, A., Oppelstrup, T. & Bulatov, V. V. Probing the limits of metal plasticity with molecular dynamics simulations. *Nature* **550**, 492–495 (2017).
33. Lu, Y., Huang, J. Y., Wang, C., Sun, S. & Lou, J. Cold welding of ultrathin gold nanowires. *Nat. Nanotechnol.* **5**, 218–224 (2010).

Acknowledgements A.S. acknowledges funding from the European Union's H2020 Framework Programme/ERC Starting Grant agreement number 637748 – NanoSOFT. L.B. acknowledges funding from the European Union's H2020 Framework Programme/ERC Advanced Grant – Shadoks.

Reviewer information *Nature* thanks Erio Tosatti and the other anonymous reviewer(s) for their contribution to the peer review of this work.

Author contributions A.N., L.B. and A.S. conceived and supervised the project. A.S. and A.N. designed the experiments. J.C. developed the experimental setup. J.C. and A.L. performed the experiments. J.C. wrote the manuscript with input from all the authors.

Competing interests The authors declare no competing interests.

Additional information
Extended data is available for this paper at https://doi.org/10.1038/s41586-019-1178-3.
Reprints and permissions information is available at http://www.nature.com/reprints.
Correspondence and requests for materials should be addressed to A.S.
Publisher's note: Springer Nature remains neutral with regard to jurisdictional claims in published maps and institutional affiliations.

METHODS

Experimental setup. Gold wires were obtained from Goodfellow (200 μm diameter, 99.99% purity). The wire was glued to the electrode on one prong of the tuning fork using conductive epoxy glue, and cut using a wire cutter. Gold substrates were obtained by evaporating a 5-nm-thick chromium layer and a 150-nm-thick gold layer on Si/SiO_2 substrates. In all experiments, a bias of 13 mV was applied to the gold substrate with respect to the grounded gold tip, allowing measurement of the junction conductance G. In our rheological measurements (Fig. 2, Extended Data Fig. 5), the mean junction conductance was kept to a fixed value using an additional proportional integral control loop on the substrate position to compensate for residual thermal drift. All experiments were performed at room temperature. Experiments presented in the main text were performed in a nitrogen atmosphere, with desiccants used to keep the humidity level below 5% relative humidity. At the beginning of the experiments, the tip was gently indented on the substrate to create a clean metallic gold contact. Force spectroscopy measurements at large oscillation amplitude (Extended Data Fig. 3) were performed in a vacuum chamber at a pressure of 10^{-6} mbar.

Measurement of viscoelastic properties. To probe the mechanical properties of the junction, we excited the tuning fork via a piezo dither, with a periodic force $F^* = Fe^{i\omega t}$, leading to subnanometric oscillations $a^* = ae^{i\omega t + \phi}$ of the tuning fork and upper gold electrode. The viscoelastic behaviour of the gold nanojunction can be characterized by the complex impedance[34] $Z^* = F^*/a^* = (F/a)e^{-i\phi}$. The real part $Z' = \mathrm{Re}(Z^*)$ characterizes the elastic response of the junction, and leads to a shift $\delta\omega$ of the tuning-fork resonance frequency as $Z' = 2k_{TF}\delta\omega/\omega_0$, with $k_{TF} = 40$ kN m^{-1} the tuning fork stiffness and $\omega_0/2\pi \approx 31$ kHz the free resonance frequency (the shift of the resonance frequency was measured via a phase-locked loop). The imaginary part $Z'' = \mathrm{Im}(Z^*)$ characterizes the dissipative response of the junction and can be measured by tracking the piezo excitation force F necessary to keep the oscillation amplitude of the tuning fork constant[35] (using a proportional integral loop). We show in Extended Data Fig. 1 the raw data for the frequency shift δf and excitation E of the tuning fork as a function of oscillation amplitude a (in picometres) (red curves correspond to a tuning fork oscillating far from the substrate in the absence of interactions, and blue curves correspond to a metallic gold contact). To obtain the dissipative mechanical impedance associated with the junction, we fit the initial linear relation between the excitation voltage E_{lin} and the oscillation amplitude a_{lin} to obtain the intrinsic dissipation of the tuning fork (plus possible additional contact contributions) such that $E_{lin} = Ca_{lin}$. In this linear regime, we can relate the excitation force F_{lin} of the piezo dither (proportional to the excitation voltage E_{lin}) to the free quality factor Q_0 of the tuning fork as $F_{lin} = k_{TF}\, a_{lin}/Q_0$. We then extract the intrinsic dissipative impedance $Z''(a)$ of the gold junction for the oscillation a of the tuning fork as $Z''(a) = k_{TF}\{[E/(Ca)] - 1\} = k_{TF}\{[E(a)/E_{lin}(a)] - 1\}$.

Geometry of the junction. The constant elastic stiffness Z'_0 in the elastic regime (Fig. 2a, green) allows a coarse characterization of the geometry of the junction. Modelling the junction as a short cylinder with area $A = N\pi d_{gold}^2/4$ with N the contact number and $d_{gold} = 0.288$ pm the atomic diameter of gold, we express the junction stiffness as $Z'_0 = E_{gold}A/h$ with E_{gold} the elastic modulus and h an equivalent cylinder height (Fig. 1b)[11]. Taking the Young modulus of bulk gold as $E_{gold} = 79$ GPa, we extract the contact height h, which is found typically in the range $h \approx 1$–6 nm.

Effect of excitation frequency on the plastic transition. To further probe the dependence of the plastic transition on the excitation frequency, we used an additional piezo dither to impose an additional shearing motion to the substrate (Fig. 3d). In this configuration, the tuning fork probed the mechanical properties of the junction with a fixed oscillation amplitude $a_{TF} = 60$ pm (smaller than the critical oscillation amplitude to induce plastic flow), and the piezo dither was excited at various frequencies from 1 to 500 kHz. Experiments conducted in this configuration were performed for a contact number $N = 15$.

We show in Extended Data Fig. 2 the mechanical impedance of the junction as a function of the oscillation amplitude of the piezo dither oscillating at 200 kHz. We recover a trace in the mechanical impedance similar to that in Fig. 2b, showing that the plastic transition can indeed be induced by the oscillation of the piezo dither. Owing to the absence of correlation between the tuning-fork oscillation a_{TF} and the substrate oscillation a_s, we define here the critical oscillation amplitude as $a_Y = a_{TF} + a_s^{crit}$ and measure the critical yield strain as $\varepsilon_Y = a_Y/h$ with $h = E_{gold}A/Z'_0$ and the viscosity as $\eta = Z''_\infty h/A\omega$.

Capillary attraction at large oscillation amplitude. Importantly, we observe a similar capillary-like signature for the behaviour of gold junctions when performing force spectroscopy measurements at large oscillation amplitude $a = 1$ nm in a high-vacuum environment (10^{-6} mbar). Extended Data Fig. 3 shows the approach of an oscillating gold tip to a gold substrate. Upon approach we observe a sudden jump to contact, characterized by a negative stiffness of $Z' \approx -4$ N m^{-1} (Extended Data Fig. 3a), concomitant with the apparition of a conductance of several G_0 in magnitude characterizing a metallic contact of few atoms (Extended Data Fig. 3b). Upon retraction, a hysteresis of about 1 nm is observed. This jump to contact is another signature of the liquid-like nature of the gold nanojunction at large shear rates.

Energy balance for the shear-induced fluidization of the junction. A first naive explanation for the liquid-like adhesive behaviour of the junction at large oscillation amplitude would be local frictional heating, leading to melting of the gold. To estimate this local heating of the junction, we write the increase in temperature in the junction as $A\lambda(\Delta T/h) \approx P_d$, with $P_d = Z''a^2\omega$ the power dissipated in the junction. We take conservative estimates, with $\lambda_{gold} = 314$ W m^{-1} K^{-1} corresponding to the bulk gold conductivity, a dissipated power of $P_d = 100$ eV per cycle $\approx 3.2 \times 10^{-13}$ W (Extended Data Fig. 4), a height of $h \approx 6$ nm and an area of $A \approx 0.3$ nm^2 (Fig. 2b). This leads to a local temperature increase ΔT of the order of 2×10^{-5} K, ruling out any frictional heating effects in the liquid-like behaviour of the gold nanojunction.

The adhesive liquid-like behaviour at large oscillation amplitude might thus originate in the shear-induced fluidization of the entire junction. We evaluate this possibility by balancing the work necessary to deform the junction in volume as $E_v = Ah\sigma_Y$ with the energy $2\pi Z''_\infty a^2$ injected in the junction over one oscillation cycle by the shearing motion of the tuning fork. Using our rheology measurement, we characterize the critical amplitude a_L at which a negative stiffness, characterizing the liquid character of the junction, is observed (Fig. 2b, liquid regime, blue zone; Extended Data Fig. 5). The energy dissipated in the junction per oscillation cycle at the oscillation amplitude a_L can then be estimated as $E_d = 2\pi Z''_\infty a_L^2$. Simultaneously, we can estimate the total volume V of the junction using the measurement of the cross-sectional area A (measured from the contact number N) and height h (estimated from the stiffness at low amplitude, Z'_0), such that $V = Ah$. Extended Data Fig. 4 shows that these two quantities are well correlated, with $Z''_\infty a_L^2 2\pi \approx hA\sigma_Y^L$. Using this energy balance, we find another estimate of the yield modulus as $\sigma_Y^L \approx 1.6$ GPa. We can thus attribute the observed adhesive liquid-like regime to the complete shear-induced fluidization of the junction.

Comparison with Prandtl–Tomlinson model. To get further insights into the peculiar nonlinear deformation mechanism at play in the junction, it is interesting to compare our results to a simple model based on a standard harmonically driven Prandtl–Tomlinson model, pictured in Extended Data Fig. 7a[16,36]. We model the slip along one gold plane as the relative motion of two corrugated surfaces of corrugation amplitude $U_0 \approx 3.81$ eV corresponding to the cohesive energy of gold[37], periodicity of $b \approx d_0 \approx 280$ pm and number N of potential wells (Extended Data Fig. 7b), leading to an effective interaction potential of $U(x) = NU_0\sin(2\pi x/b)$.

The dynamics of the harmonic mass-spring oscillator can be solved under a harmonic drive close to the resonance frequency (see below). We show in Extended Data Fig. 7c the effective dimensionless mechanical impedance $\tilde{Z}_{FK} = Z_{FK}/(NU_0/b^2)$ associated with the Prandtl–Tomlinson model. For low oscillation amplitudes $x \ll b$, we recover a purely elastic regime associated with $Z'_{FK} \approx NU_0/b^2$ and $Z'_{FK} \approx 0$, corresponding to the linear response of the system. As the oscillation amplitude x increases above the potential wavelength, we recover a plastic regime where two adjacent atomic planes start to slip along a well defined slip plane, characterized by the increase of the dissipative impedance Z'' and the simultaneous loss in mechanical impedance as $Z' \approx 0$ (Extended Data Fig. 7c). In the Prandtl–Tomlinson model, this regime is associated with a constant solid-like friction force $F_0 \approx NU_0/b$ (of the order of 20 nN for $N = 10$), which is necessary to slide one row of atoms over the slip plane (inset, Extended Data Fig. 7c). Importantly, this yield force corresponds to the depinning force for the upper plane and varies linearly with the number N of interacting atoms, as in Fig. 3a.

However, this constant solid-like force leads to a shear-thinning behaviour, with an impedance decreasing with oscillation amplitude x as $Z'' \approx F_0/x$ (Extended Data Fig. 7b). The Prandtl–Tomlinson model thus does not predict a constant dissipative modulus Z'' for large deformation (associated with viscous-like dissipation), in strong contrast to the experimental findings of Figs. 2b, 4. In other words, Prandtl–Tomlinson-like models, although successful in capturing atomistic friction experiments[38] and the slip of perfect crystalline interfaces[15] (Fig. 3c) are unable to capture the experimental observation of a viscous-like fluidization of the molecular junction (Fig. 4).

Simulation procedure. We follow refs. [16,36] and describe the motion of the harmonically driven oscillator subjected to a periodic potential as $M\ddot{x} + \gamma\dot{x} + Kx + \frac{U_0}{2\pi b}\sin(2\pi x/b) = F_{ext}\sin(\omega t)$ where M (in kilograms), γ (in kilograms per second) and K (in newtons per metre) are the effective mass, damping and spring constant of the oscillator, respectively, U_0 (in joules) is the barrier height, b (in metres) is the corrugation size and F_{ext} (in newtons) is the external oscillatory forcing. The free oscillator can be characterized by its quality factor $Q = M\omega_0/\gamma$ (non-dimensional) and resonance frequency $\omega_0 = \sqrt{K/M}$ (in hertz).

After non-dimensionalization, we obtain $\tilde{\omega}^2\ddot{X} + \frac{\tilde{\omega}}{Q}\dot{X} + X + \alpha\sin(2\pi X) = \tilde{F}\sin(2\pi t)$, where we define the dimensionless displacement $X = x/b$, the force

$\widetilde{F} = F_{ext}/M\omega_0^2$, the dimensionless driving frequency $\widetilde{\omega} = \omega/\omega_0$ and $\alpha = U_0/d_0^2K$, which characterizes the importance of the typical stiffness of the corrugation over the probe stiffness. We define the dimensionless mechanical impedance $\widetilde{Z}$ and the dimensionless dissipative force $\widetilde{F}_D$ as $\widetilde{Z} = \frac{Z}{U_0/d_0^2}$ and $\widetilde{F}_D = \frac{F_D}{U_0/d_0^3}$, respectively.

To obtain numerically the variation in Z' and Z'', we numerically determine the motion of the oscillator under a periodic forcing, with a perturbative periodic potential $\alpha = 0.05$. We can extract the quality factor Q at resonance and the centre frequency of the resonance ω_r from the variation of the phase ϕ of the oscillator close to resonance, as $1/\tan\phi \approx -2Q\left(\frac{\widetilde{\omega}-\widetilde{\omega}_r}{\widetilde{\omega}_r}\right)$. From the measurements of ω_r, we extract the dimensionless storage modulus $\widetilde{Z}' = \frac{2}{\alpha}(\widetilde{\omega}_r - \widetilde{\omega}_0)$. We express the dimensionless loss modulus $\widetilde{Z}''$ as a function of the quality factor as $Z'' = \frac{1}{\alpha}\left(\frac{1}{Q} - \frac{1}{Q_0}\right)$.

Data availability

The data shown in the plots and other findings of this study are available from the corresponding author upon reasonable request.

34. Comtet, J. et al. Nanoscale capillary freezing of ionic liquids confined between metallic interfaces and the role of electronic screening. *Nature Mater.* **16**, 634–639 (2017).
35. Comtet, J. et al. Pairwise frictional profile between particles determines discontinuous shear thickening transition in non-colloidal suspensions. *Nat. Commun.* **8**, 15633 (2017).
36. Zaloj, V., Urbakh, M. & Klafter, J. Deducing energy dissipation from rheological response. *J. Chem. Phys.* **110**, 1263–1266 (1999).
37. Kittel, C. *Introduction to Solid State Physics* 7th edn, Vol. 8 (Wiley, New York, 1996).
38. Bylinskii, A., Gangloff, D. & Vuletić, V. Tuning friction atom-by-atom in an ion-crystal simulator. *Science* **348**, 1115–1118 (2015).

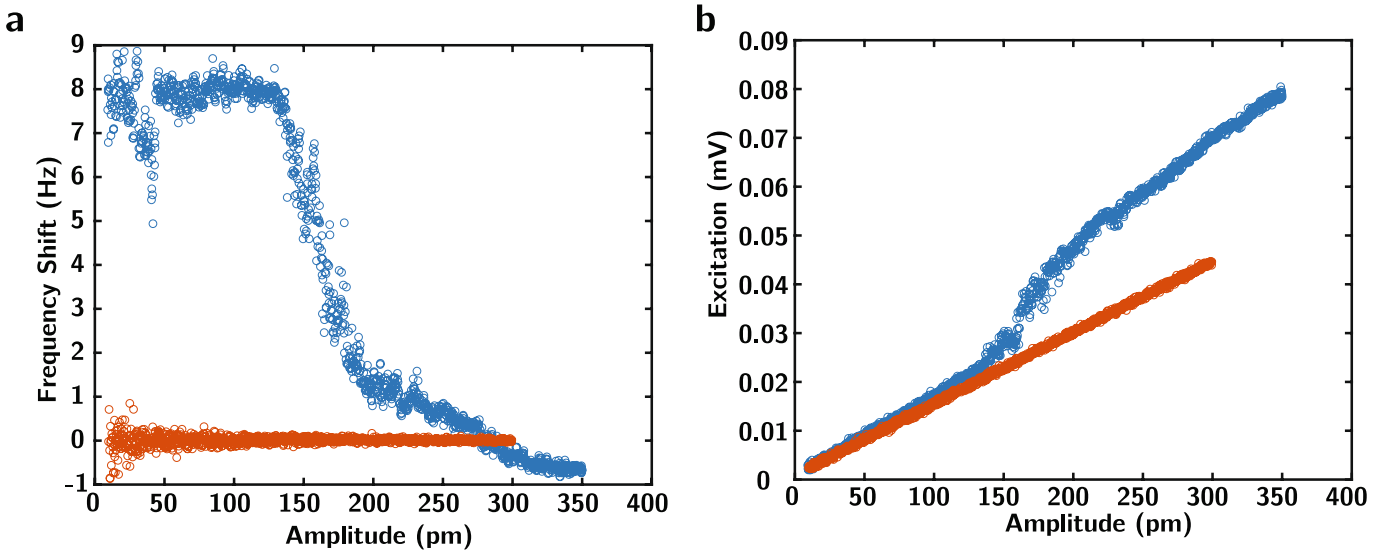

Extended Data Fig. 1 | Raw data. a, **b**, Raw data showing the frequency shift $\delta f = \delta\omega/2\pi$ (**a**) and the excitation voltage E (**b**) far from the substrate (red curves) and during a typical rheological experiment on a metallic gold contact ($N = 11$) (blue).

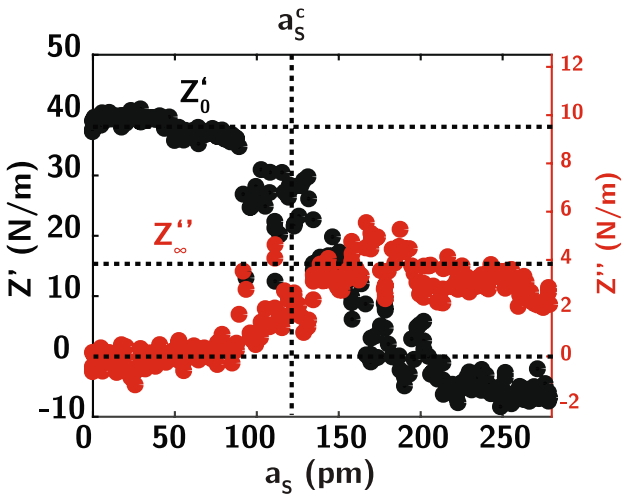

Extended Data Fig. 2 | Effect of excitation frequency on the plastic transition. Mechanical impedance Z' and Z'' of the gold junction as a function of oscillation amplitude a_s of the substrate with $f_s = 200$ kHz. Entry in the plastic regime occurs at the critical substrate oscillation amplitude a_s^c. Cross-sectional atom number is $N = 15$.

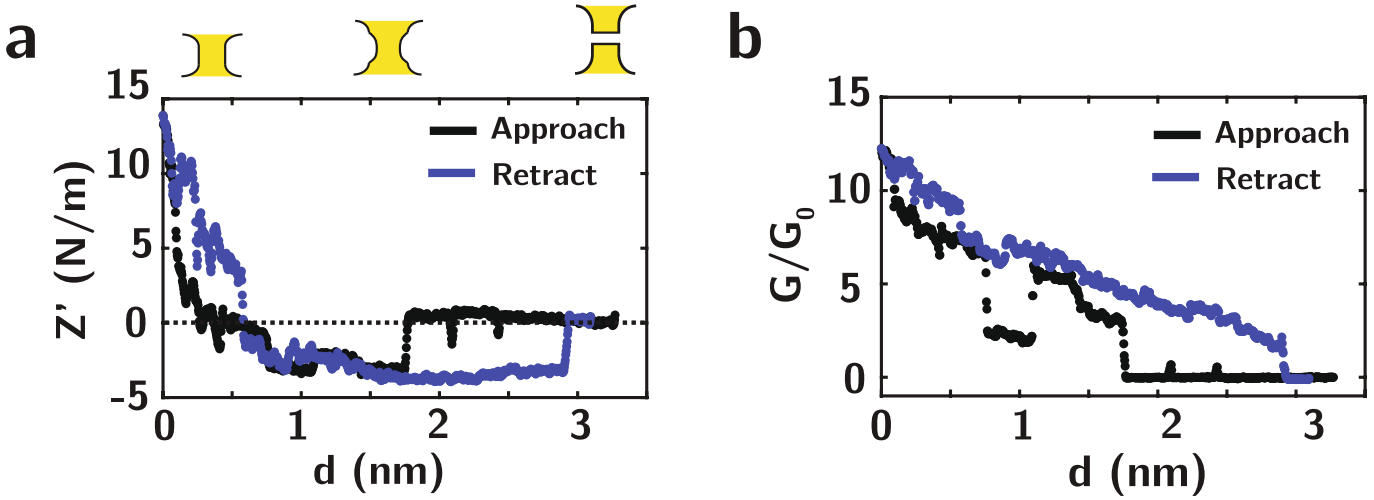

Extended Data Fig. 3 | Force spectroscopy at large oscillation amplitude. a, **b**, Force spectroscopy showing the approach (black) and retraction (blue) of the gold tip to the gold substrate at large oscillation amplitude (1 nm) for the conservative mechanical impedance Z' (**a**) and the dimensionless conductance G/G_0 (**b**).

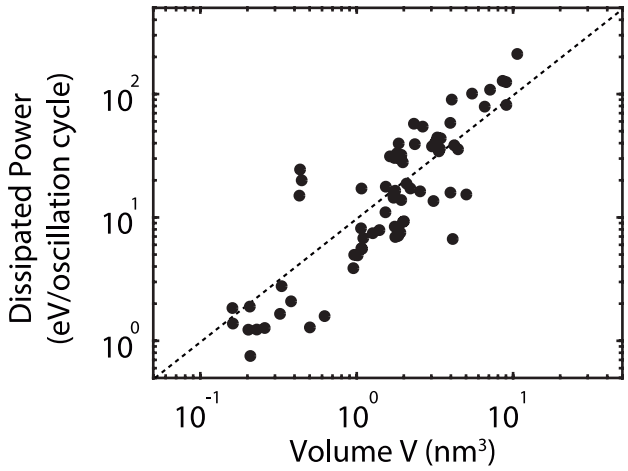

Extended Data Fig. 4 | Energy balance for the shear-induced fluidization of the junction. Dissipated energy in the junction over one oscillation cycle as a function of melted volume (see Methods for details). The dashed line has a slope of 1.

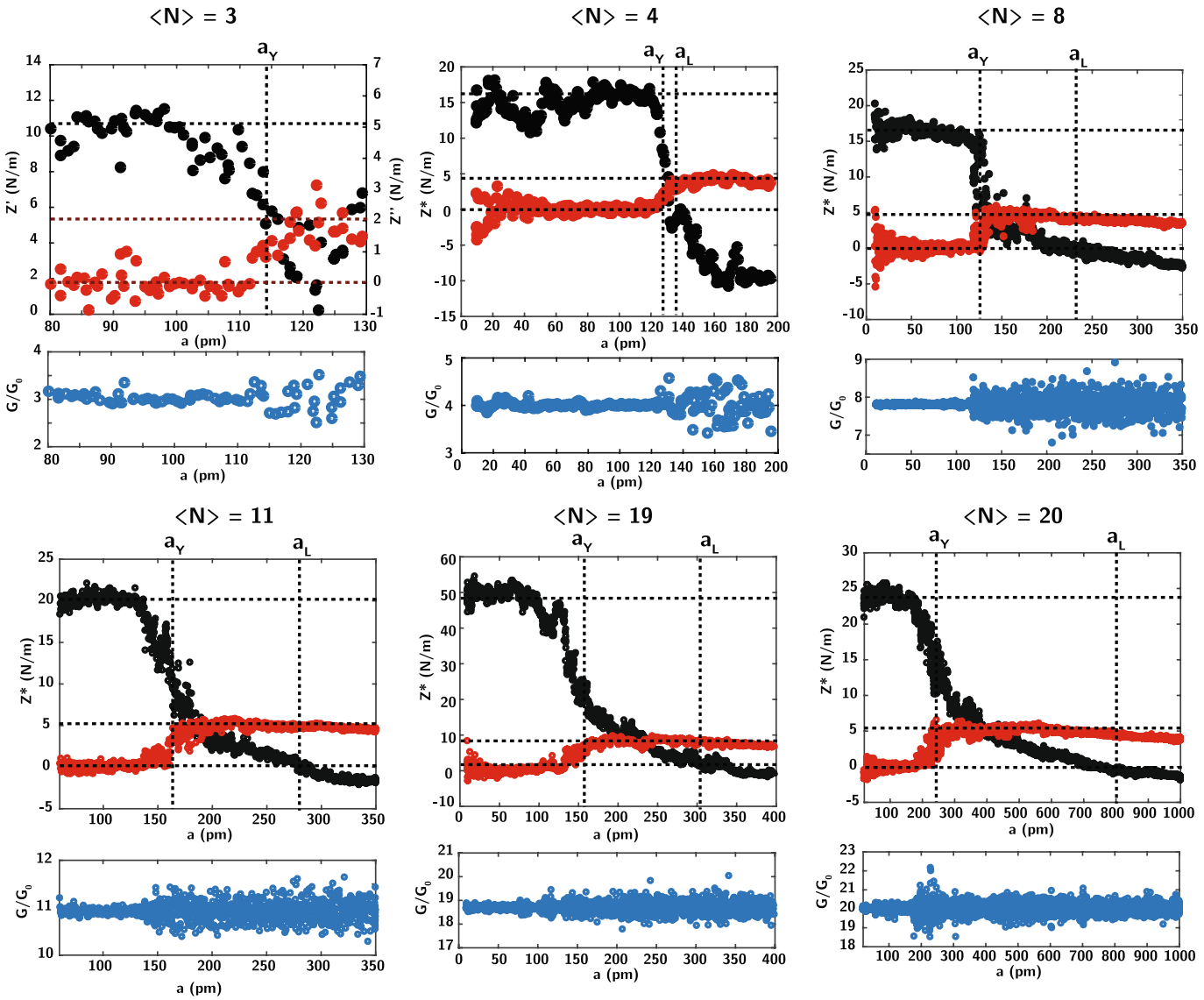

Extended Data Fig. 5 | Typical rheological curves. Typical rheological curves for various contact conductances, showing the conservative modulus Z' (black), the dissipative modulus Z'' (red) and the mean current (blue). The general trends of the rheological curves are maintained, with: (1) a plastic transition at a critical oscillation amplitude a_Y, corresponding to a decrease in Z', an increase in Z'' and an increase in current fluctuations; (2) a plateau in the dissipative impedance at large oscillation amplitude; and (3) a decrease in the conservative impedance to negative values $Z' < 0$, corresponding to a capillary-like attraction at a critical oscillation amplitude a_L.

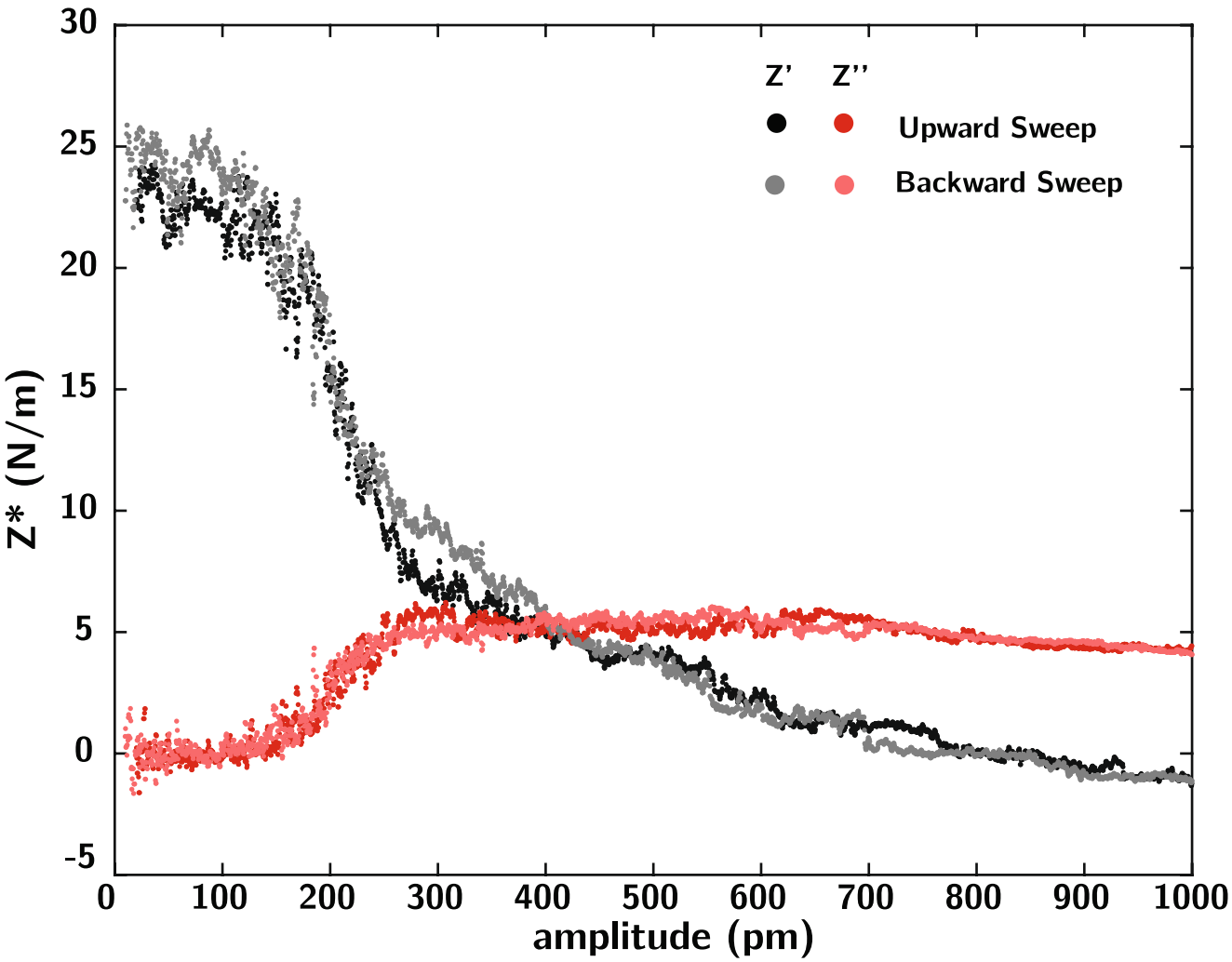

Extended Data Fig. 6 | Reversibility of the plastic transition. Rheological curve obtained for increasing (dots) and decreasing (cross) oscillation amplitude (here for $N = 20$). The plastic transition is found to be completely reversible, with negligible hysteresis.

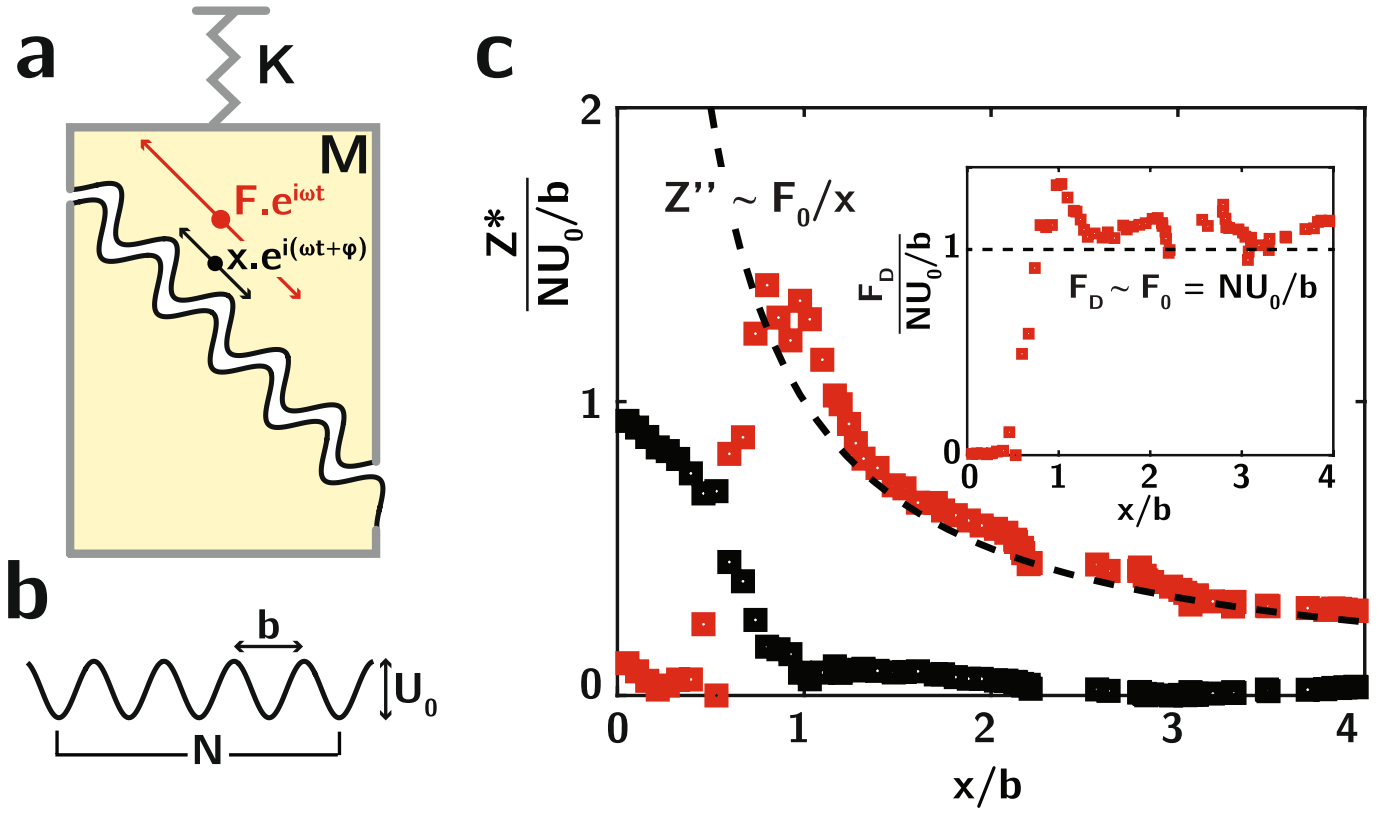

Extended Data Fig. 7 | Prandtl–Tomlinson model. a, **b**, Schematic of the model, with a mass-spring oscillator of mass M and stiffness K (**a**) interacting with a corrugated potential of N potential wells of corrugation energy U_0 and corrugation period b (**b**). **c**, Simulation results, showing the dimensionless dissipative and conservative impedance $\widetilde{Z} = Z/(NU_0/b)$ as a function of dimensionless oscillation amplitude x/b. Inset, dimensionless dissipative force, $F_D/(NU_0/b)$.